



# Effect of anolytic nitrite concentration on electricity generation and electron transfer in a dual-chamber microbial fuel cell

Rongchang Wang<sup>1</sup> · Xuehao Wang<sup>1</sup> · Xinyi Zhou<sup>1</sup> · Jiabin Yao<sup>1</sup>

Received: 24 July 2019 / Accepted: 5 December 2019 / Published online: 11 January 2020  
© Springer-Verlag GmbH Germany, part of Springer Nature 2020

## Abstract

This study reports the effect of anolytic nitrite concentration on electricity generation and electron transfer in microbial fuel cells (MFCs). Anolytic nitrite enhanced the electricity generation capability of the MFCs at relatively low concentrations ( $< 60 \text{ mg} \cdot \text{L}^{-1}$ ) but inhibited the activity of anodic electrogenic bacteria at high concentrations. In the anode chamber of the MFC, nitrite was converted to nitrate-releasing electrons before being quickly removed through denitrification. Nitrite alone (in the absence of organic matters) could not perform as an electricity production matrix but promoted electricity production as a co-matrix in the MFC. At an influent nitrite concentration of  $60 \text{ mg} \cdot \text{L}^{-1}$ , the coulombic efficiency of the MFC was minimized at approximately 5.4%, and the charge transfer resistance was also lowest, while the concentrations of extracellular polymeric substances (EPS) and cytochrome *c* were both maximized. Higher anolytic nitrite concentrations ( $> 60 \text{ mg} \cdot \text{L}^{-1}$ ) inhibited the production of cytochrome *c* and EPS and increased the charge transfer resistance, thereby reducing the efficiency of electron transfer in the anodic biofilm. The results provide valuable guidelines for MFC applications in wastewater treatment processes with nitrite-containing influents.

**Keywords** Microbial fuel cell · Electricity generation · Nitrite removal · Extracellular polymeric substances (EPS) · Cytochrome *c*

## Introduction

Owing to their inadequate supply and adverse influence on environmental and economic development, fossil fuels will be increasingly replaced by sustainable technology in the future (Fu et al. 2018). However, the high energy cost of traditional wastewater treatment technology contradicts the trend of sustainable development (McCarty et al. 2011; Oh et al. 2010). Accordingly, sustainable energy production and new water treatment technology research have become prime concerns of the twenty-first century. Microbial fuel cell (MFC) is a sustainable wastewater

treatment technology that consumes diverse organic substrates as fuel (Logan and Regan 2006; Viridis et al. 2010). By chemically reacting with oxygen or other reagents, an MFC converts the chemical energy from contaminants into electricity, thereby performing dual roles of pollutant treatment and energy recovery. The various wastewaters used as MFC substrates for electricity generation and wastewater treatment include domestic sewage (Park et al. 2018), swine wastewater (Ding et al. 2017), and leachate (Moharir and Tembhurkar 2018). These usages have highlighted the wide application potential of MFCs in wastewater treatment.

In addition to consuming organic matters to generate electricity, MFCs utilize substances such as nitrite, which react as biocathodic electron acceptors. Therefore, MFCs promise to simultaneously remove both organic carbon and nitrite from wastewater (Al-Mamun et al. 2017). Faraghi and Ebrahimi (2012) successfully operated a microbial fuel cell using nitrite as the anodic electron donor. They concluded that nitrite can be oxidized to nitrate in the absence of  $\text{O}_2$ , providing a possible substrate for electricity generation in MFCs. Chen et al. (2014) reported that besides the primary nitrification substrate (ammonium), the intermediates (hydroxylamine and nitrite) supply anodic fuel for current generation.

Responsible editor: Bingcai Pan

**Electronic supplementary material** The online version of this article (<https://doi.org/10.1007/s11356-019-07323-z>) contains supplementary material, which is available to authorized users.

✉ Rongchang Wang  
wangrongchang@tongji.edu.cn

<sup>1</sup> Institute of Biofilm Technology, Key Laboratory of Yangtze Aquatic Environment (MOE), State Key Laboratory of Pollution Control and Resource Reuse, College of Environmental Science and Engineering, Tongji University, Shanghai 200092, China

Nitrite is an important intermediate product in nitrogen contaminant removal. It can either be reduced to NO or N<sub>2</sub>O through denitrification or oxidized to nitrate by nitrite-oxidizing bacteria (NOB). Ma et al. (2017) reported that NOB induces the release of electrons from nitrite. Therefore, a certain amount of nitrite can be detected in several raw wastewaters or their treated effluents. Hence, before treating actual nitrite-containing wastewater by MFC technology, we must further investigate the influence of nitrite on electricity generation, pollutant degradation, or some other performance of MFC. Current investigations have focused on the degradation of organic compounds and the reduction of nitrogenous compounds in the anode and cathode chamber of MFCs, respectively. However, the transformation and degradation of nitrite in the anode chamber of MFCs has not been fully explored. The effects of nitrite on the performance of MFCs, and its mechanism in the MFC, are unavoidable problems in practical applications.

To resolve these problems, this study investigates the effect of anolytic nitrite concentration on the electricity production capacity and contaminant removal efficiency of dual-chamber MFCs with sodium acetate as the electron donor in continuous flow mode. The results provide a theoretical basis and technical support for the MFC treatment of actual nitrite-containing wastewater.

## Materials and methods

### MFC configuration and operation

The two-chambered microbial fuel cell (MFC; anode and cathode chambers of net volume 302 mL each) was constructed from plexiglass. The chambers were separated by a proton exchange membrane (Nafion™ 117, DuPont, USA) (Fig. 1). The anode and cathode electrodes were constructed from carbon felt (diameter 5 cm) with a 20-cm<sup>2</sup> working area. The anolyte was deoxygenated with N<sub>2</sub> for 10 min to maintain an anaerobic condition. Experiments were carried out in an anaerobic chamber to prevent O<sub>2</sub> interference with the nitrite degradation. The anode compartment was inoculated with the effluent from the MFC running on acetate. All experiments were conducted at 23 ± 2 °C. The MFC was operated under a constant load of 1000 Ω.

Five MFCs were set up and run in batch mode for inoculation. The output voltage of each MFC reached approximately 0.13 V after about 5 days, indicating that some microbes had already attached and proliferated on the anode carbon felt. The operation mode was then changed to continuous flow with nutrient solutions of different concentrations (0 to 120 mg·L<sup>-1</sup>). The cell voltage resistance was measured across a 1000 Ω resistor. The hydraulic retention time (HRT) was 50 h under continuous flow.

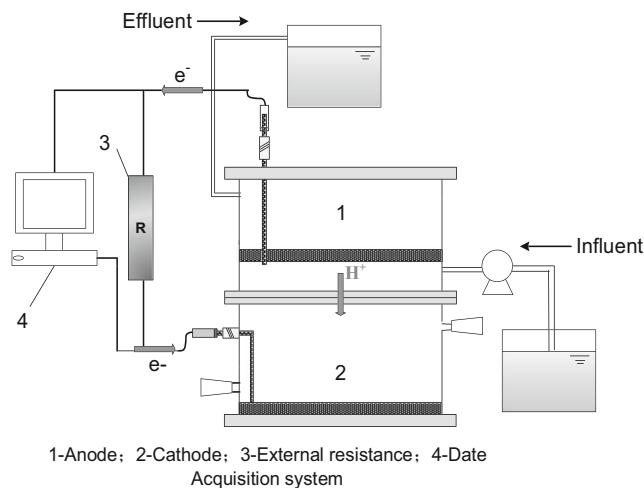


**Fig. 1** Schematic of the MFC system. The synthetic medium was fed to the anode by a peristaltic pump (HRT = 50 h). The external resistance was 1000 Ω. The cell voltage was recorded every 5 min by a data acquisition system

The MFC was operated using synthetic analytes with the following composition (grams per L deionized water): C<sub>2</sub>H<sub>3</sub>NaO<sub>2</sub>·3H<sub>2</sub>O 2.127, K<sub>2</sub>HPO<sub>4</sub>·3H<sub>2</sub>O 18.3, KH<sub>2</sub>PO<sub>4</sub> 2.7 (pH = 6.8–8.8, buffer capacity = 0.0366 mol·L<sup>-1</sup>·pH<sup>-1</sup>), NH<sub>4</sub>Cl 0.1, NaCl 0.5, MgSO<sub>4</sub>·7H<sub>2</sub>O 0.1, CaCl<sub>2</sub>·2H<sub>2</sub>O 0.015 (Virdis et al. 2012), trace elements 1 ml (Lu et al. 2006). The initial COD concentration in the anolyte was around 1200 mg·L<sup>-1</sup>; the detailed initial COD concentrations were presented in Table 1. Different nitrite concentrations (initial nitrite-*N* = 0, 30, 60, 90, and 120 mg·L<sup>-1</sup>) were added to the anode in different reactors. The cathode chamber was filled with 50 mM potassium ferricyanide solution and pH was kept at 7.4 to minimize the influence of the cathode potential on the overall cell performance.

### Data acquisition, electrochemical and chemical measurements

The cell voltage was recorded every 5 min by a data acquisition module (KEITHLEY 2700, Keithley Company, USA), and the current *I* (A) was calculated by Ohm's law:

$$I = E_{\text{cell}}/R_{\text{ext}} \quad (1)$$

where *E*<sub>cell</sub> is the output voltage (V), and *R*<sub>ext</sub> is the external resistance (Ω).

The sodium acetate concentration was calculated in terms of COD and measured by standard methods (APHA et al. 1998). The nitrite and nitrate concentrations were measured colorimetrically (APHA et al. 1998).

All measurements were conducted in triplicate, and the results are expressed as their means ± standard deviations. The significance of the results was tested by analysis of

**Table 1** COD removal and Coulombic efficiency of MFCs at different anolytic nitrite concentrations

Nitrite concentration (mgN·L <sup>-1</sup> )	Initial COD (mgN·L <sup>-1</sup> )	COD removal (%)	COD removal loading (g COD m <sup>-2</sup> ·d <sup>-1</sup> )	Coulombic efficiency (%)	Power density (mW·m <sup>-2</sup> )
0	1180 ± 13	34.7 ± 2.3	29.8 ± 2.8	7.8 ± 0.7	208.3 ± 2.9
30	955 ± 25	39.0 ± 5.2	27.1 ± 4.5	9.5 ± 1.1	263.2 ± 3.9
60	1217 ± 16	53.5 ± 1.9	47.8 ± 3.1	5.4 ± 0.9	266.5 ± 1.3
90	1165 ± 19	31.9 ± 2.9	27.4 ± 3.2	7.5 ± 1.3	138.2 ± 3.0
120	1209 ± 34	25.2 ± 3.2	22.2 ± 3.7	6.9 ± 0.8	103.8 ± 1.1

variance (ANOVA) in SPSS Statistics 17.0, with statistical significance designated by  $p < 0.05$ .

### Coulombic efficiency(CE)

Coulombic efficiency (CE) is the ratio of the total number of electrons transferred to the anode from the substrate to the maximum possible number of electrons if all substrate removal could produce a current. In the continuous flow scenario, the Coulombic efficiency depends on the current generated under steady conditions as shown in Eq. (2):

$$CE = \frac{MI}{Fbq\Delta COD} \quad (2)$$

where  $M=32$  is the molecular weight of oxygen,  $F$  is Faraday's constant,  $b=4$  is the number of electrons exchanged per mole of oxygen,  $q$  is the volumetric influent flow rate, and  $\Delta COD$  is the difference between the influent and effluent CODs. Again, the current  $I$  was calculated by Ohm's law (Logan and Regan 2006).

### Electrochemical impedance spectroscopy(EIS)

Electricity generation and power density are related to the electron transfer or charge transfer, where the latter relates to the internal resistance (Kim et al. 2014). The internal resistance was analyzed by electrochemical impedance spectroscopy (EIS) on an electrochemical workstation (CHI660E, Chenhua Instrument Inc., Shanghai, China). The frequency was ranged from 0.01 Hz to 100 kHz on the whole cell (two-electrode mode) (Barsoukov and Macdonald 2005). An EIS spectrum typically comprises a semicircle and a linear portion representing the ohmic resistance, charge transfer resistance, and diffusion resistance, respectively (Katz and Willner 2003). The first intersection on the x-axis of the EIS spectrum represents the ohmic resistance, the diameter of the first (high frequency) circle is the charge transfer resistance, and the solution resistance is found at high frequencies where the impedance data cross the Re(Z) axis (Borole et al. 2010; Hutchinson et al. 2011). The ohmic resistance is contributed by the electrodes, solutions, membranes, and interfaces. The

charge transfer resistance represents the capacitance and polarization resistance built on the electrical double layer of the electrode surfaces (Kim et al. 2014). The Nyquist plots of the EIS spectra were analyzed using Zview Software.

### EPS and cytochrome *c*

Extracellular polymeric substances (EPS) and cytochrome *c* may assist electron transfer through biofilms (Cao et al. 2011; Gralnick and Newman 2007). To explore its effect on the anode microbial biofilm, the influent nitrite concentration was varied in the present study, and the EPS and cytochrome *c* contents on the anode electrode were determined.

The biofilm EPS in each reactor was extracted and determined as described in Fang et al. (2002). When the output power reached stability, biofilm-coated samples were removed from each MFC and immersed in 50 mL of TE buffer (pH 7.5) containing 10 mM Trizma base, 10 mM EDTA, and 2.5% NaCl. Biofilm was scraped from each sample and centrifuged at 4000 rpm for 20 min. For EPS extraction, the concentrated biomass was resuspended in 10 ml of a 0.85% sodium chloride solution containing 0.22% formaldehyde at 80 °C for 30 min. The EPS dissolved in the formaldehyde solution was recovered by further centrifugation at 3500 rpm for 30 min. The carbohydrate and protein contents of EPS in the extracted solution were measured by the phenol/sulfuric acid method (Gaudy 1962) and the Lowry method (Lowry et al. 1951), respectively, and were summed to obtain the total EPS of the samples. Calibration curves for determining the EPS carbohydrates and proteins were constructed using lactose and bovine serum albumin, respectively.

As heme is a constituent of cytochrome *c*, the cytochrome *c* content in the present experiment was assayed by measuring the heme concentration (Sun et al. 2014). To quantify the cytochrome *c*, small pieces of anode electrode with biofilm were taken from the MFC and immersed in phosphate buffer saline (PBS). The heme dissolved in the PBS solution was recovered by further centrifugation at 15000 rpm for 15 min at 4 °C and quantified by measuring the supernatant at 400 nm. The extraction and determination processes of heme are specified in the literature (Sinclair et al. 2001).

### Scanning electron microscopy (SEM) characterization and confocal laser scanning microscopy (CLSM)

As microorganisms crucially affect the performance of MFCs, the biofilm morphology was clarified by scanning electron microscopy (SEM) (3400 N, HITACHI instrument) and confocal laser scanning microscopy (CLSM) (Leica TCS SP5, Germany). For SEM analysis, anode biofilm pieces were sampled from each MFC and washed twice with sterilized PBS solution. The anode pieces were fixed by immersion in 3% glutaric dialdehyde for 10 h at 4 °C. The residual glutaric dialdehyde was removed from the anode samples by three 20-min washes with PBS. The anode samples were then dehydrated by sequential treatment with a series of ethanol dilutions (30%, 50%, 70%, 90%, and 100%), each applied for 20 mins. Finally, the samples were mounted on metal stubs and coated with gold. The biofilm was observed in high vacuum using the secondary electron imaging mode of SEM.

Images of the biofilms cultured in the MFC anode were nondestructively obtained by CLSM. Parameters such as biofilm depth and cell area (biomass) were determined by digital image analysis of the CLSM optical thin sections at various depths. The proprietary staining kit LIVE/DEAD was obtained from Molecular Probes Inc. (Eugene, OR, USA) and applied as described by the manufacturer. Briefly, the LIVE/DEAD stain stored at -20 °C was warmed to room temperature and centrifuged. The staining solution contained 10 mL of deionized water and 15 µL each of the two components A and B. This working solution was applied directly to the biofilms for 15 min. The stained samples were detected under CLSM and analyzed with Image J software.

## Results and discussion

### Electricity generation and power density

The required start-up time was shorter for reactors supplied with low nitrite concentrations (0–60 mg·L<sup>-1</sup>) than for reactors with relatively high nitrite concentrations (90 and 120 mg·L<sup>-1</sup>) (11 days to stable voltage in the former case versus ~ 27 days in the latter; see Fig. 2). Therefore, it was concluded that increasing the analytic nitrite concentration extended the start-up time of the MFC. In addition, as shown in Fig. 2, the stable voltage outputs in the nitrite and no-nitrite cases were obviously different. The stable output voltages of the MFC were 0.72 ± 0.02 V and 0.73 ± 0.03 V in the presence of 30 and 60 mg·L<sup>-1</sup> nitrite, respectively, and 0.65 ± 0.03 V in the control reactor (nitrite concentration 0 mg·L<sup>-1</sup>). This suggests that low nitrite levels (0–60 mg·L<sup>-1</sup>) raised the system voltage. At very high nitrite concentrations, the recorded peak voltage outputs were suppressed (0.52 ± 0.01 V and 0.46 ± 0.02 V at 90 and 120 mg·L<sup>-1</sup>, respectively).

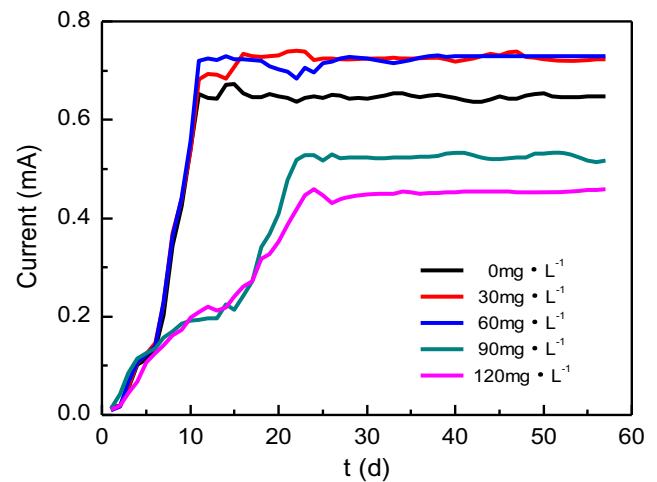


Fig. 2 Current output of MFCs at different analytic nitrite concentrations (external resistance = 1000 Ω, HRT = 50 days)

Based on these results, we hypothesize that low nitrite concentration promotes electricity generation in the system, enhancing the maximum output voltage by approximately 14%. When the nitrite concentration increased to 90 and 120 mg·L<sup>-1</sup>, the basically stable voltage output of the systems reached only around 0.50 ± 0.02 V, indicating that the anode-electrogenic bacterium of our system has limited tolerance to nitrite.

Faraghi and Ebrahimi (2012) reported that nitrite performs as an electricity generation matrix. Specifically, it contributes electricity by transferring electrons to the anode during the nitrite-to-nitrate conversion. To verify whether nitrite can act as a single matrix for electricity generation, we replaced the influent with solution containing 60 mg·L<sup>-1</sup> nitrite alone, excluding the organic matter.

The voltage output change after replacing the anode solution is shown in Fig. 3. The output voltage of the MFC

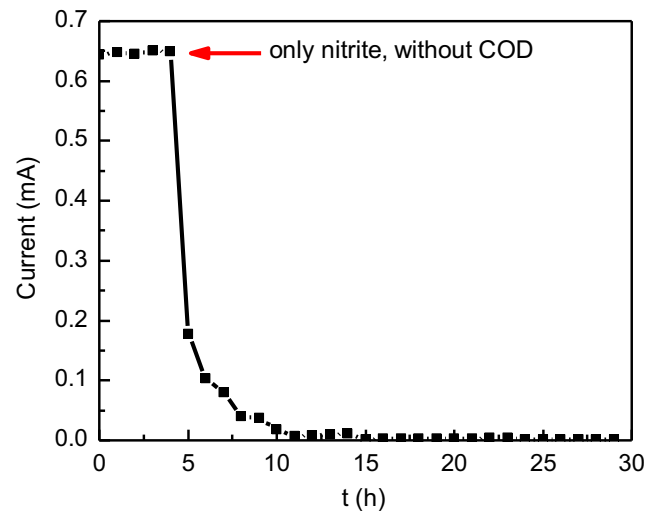


Fig. 3 Current output of MFC at a nitrite concentration of 60 mg L<sup>-1</sup> and no acetate in the analytic solution (arrowhead indicates substrate replacement)

**Table 2** Nitrogen removal from MFCs at different anolytic nitrite concentrations

Influent nitrite (mg·N·L <sup>-1</sup> )	Effluent nitrate (mg·N·L <sup>-1</sup> )	Effluent nitrite (mg·N·L <sup>-1</sup> )	Nitrite removal efficiency (%)	Nitrite loading (gN·m <sup>-2</sup> ·d <sup>-1</sup> )
0	2.51 ± 0.23	0	/	/
30	3.75 ± 0.41	4.71 ± 0.24	84.3 ± 0.8	1.83 ± 0.17
60	2.54 ± 0.17	9.33 ± 0.95	84.5 ± 1.6	3.67 ± 0.07
90	3.13 ± 0.22	12.41 ± 0.74	86.2 ± 0.8	5.62 ± 0.15
120	2.87 ± 0.38	15.74 ± 1.21	86.9 ± 1.0	7.56 ± 0.11

decreased rapidly after the replacement, reaching substantially zero after approximately 5 h. We speculated that in the initial stage after replacement, the wall surface of the reactor or carbon felt retained some organic matters, which were consumed by the electrogenic bacteria to produce electricity. When the residual organic matter was depleted, the system ceased its electricity production because nitrite alone cannot be exploited as an electricity production matrix. In the present system, nitrite cannot be a single matrix that drives the MFCs, but at certain concentrations and complemented by organic matters, it promotes their electricity production.

### Coulombic efficiency

The coulombic efficiencies of the MFC reactors at different influent nitrite concentrations are shown in Table 1. At a nitrite concentration of 60 mg·L<sup>-1</sup>, the coulombic efficiency of the system was only 5.4 ± 0.9%, much lower than under other conditions. When supplied at this concentration, the nitrite raised the speed of organic consumption, but only around 5.4% of the organic matter was expended in electrical energy production. The vast majority of the remaining organic matter was consumed by other metabolic activities of the microorganisms.

We speculated that the larger current also promoted the metabolism of the microorganisms without enabling their electricity generation. The inoculated anode bacteria were probably mixed microorganisms, most of which could not generate electricity. As such bacteria consume more organic matters than electrogenic bacteria, the coulombic efficiency

was reduced. Electron loss caused by denitrification, which also consumes organic matters, will also affect the coulombic efficiency of the system at high influent nitrite concentrations.

### COD and nitrogen removal

At all influent nitrite concentrations, the nitrite removal rates of the MFCs exceeded 80%, and no significant nitrate was accumulated in the effluents (Table 2). This result shows that most of the nitrite was removed in our system. As the influent nitrite concentration increased, the system maintained its high nitrite removal rate. The highest nitrite loading was 7.56 ± 0.11 g·m<sup>-2</sup>·d<sup>-1</sup>. It is presumed that increasing the initial nitrite concentration strengthens the NOB activity, maintaining the nitrite removal rate of the system at a high level (Magnussen and Hjertager 1981). The maximum COD removal efficiency about 53.5 ± 1.9% was observed when the nitrite concentration was 60 mg·L<sup>-1</sup>, and the maximum COD removal load reached 47.8 ± 3.1 g COD m<sup>-2</sup>·d<sup>-1</sup> (Table 1).

Relatively higher nitrite removal (84.3%–86.9%) and higher power density of 266.5 mW·m<sup>-2</sup> were achieved in this study, compared with the previous results reported by Faraghi and Ebrahimi (2012) with nitrite removal efficiency of 10% to 22% and power density of 37.8 μW·m<sup>-2</sup>. Nitrite removal by denitrification can proceed in two ways: the nitrite can first be converted to nitrate with the release of electrons or used as a direct electron acceptor. In the present experiment, nitrite concentrations of 30 mg·L<sup>-1</sup> and 60 mg·L<sup>-1</sup> significantly increased the electricity generation capacity of the system without significantly increasing the nitrate concentration in the

**Table 3** Ohmic resistance and charge transfer resistance (Ω) of MFCs at different anolytic nitrite concentrations

Experimental stage	Anolytic nitrite concentration							
	30 mg·L <sup>-1</sup>		60 mg·L <sup>-1</sup>		90 mg·L <sup>-1</sup>		120 mg·L <sup>-1</sup>	
	Ohmic	Charge transfer	Ohmic	Charge transfer	Ohmic	Charge transfer	Ohmic	Charge transfer
Day 2	1.93	3.96	1.70	1.78	1.63	4.12	2.30	9.64
Day 10	1.30	4.50	1.52	3.46	1.55	4.73	4.92	12.58
Day 20	1.48	3.42	1.62	2.57	4.34	4.29	1.59	7.13

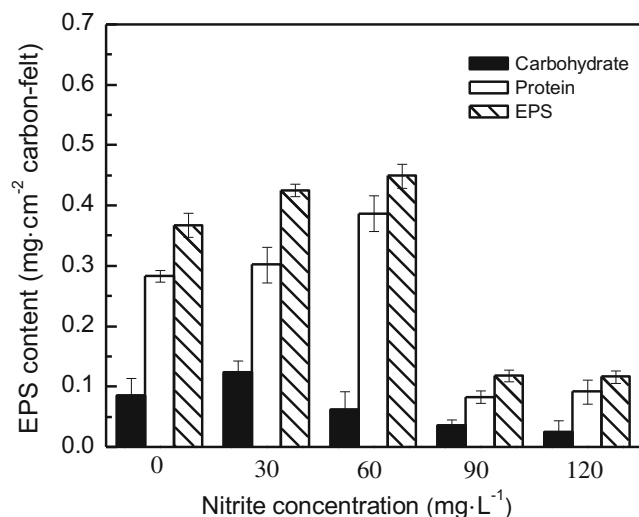


**Fig. 4** EPS contents of the anodic biofilm in MFCs at different anolytic nitrite concentrations. The sum of protein and carbohydrate represents the total EPS

effluent. This result indicates that in our system, the nitrite was quickly removed by denitrification via nitrate formation with electron release. It can be speculated that nitrite reacted as a co-matrix for electricity production. After conversion into nitrate, the nitrite was rapidly removed through a denitrification reaction in the anode chamber.

### Internal resistance and electron transfer

The internal resistance of the present system was analyzed by EIS. Nyquist plots of the whole cell on day 2, day 10, and at steady state for different nitrite concentrations together with the equivalent circuit are shown in Fig. S-1. The well-fitted EIS results simulated in Zview software are presented in Table 3.

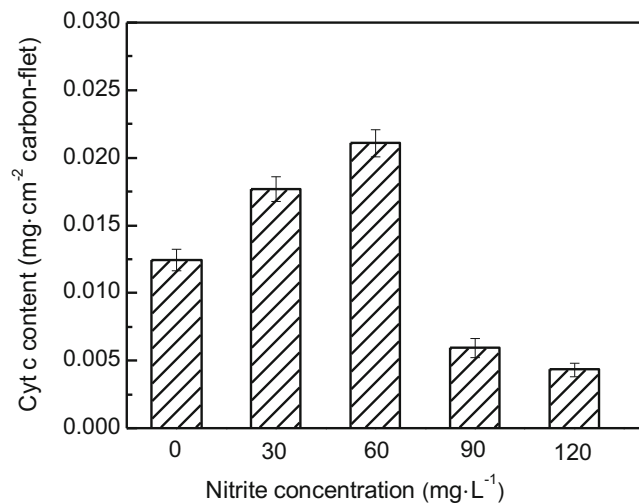


**Fig. 5** Cytochrome *c* contents of the anodic biofilm in MFCs at different anolytic nitrite concentrations

The increased voltage output in our research might be attributed to reduction of the charge transfer resistance, which was affected by the kinetics of the electrode reactions and the growth of a conductive biofilm on the electrode surface. During the stable stage of the reactors, the charge transfer resistance was lowest in the 60 mg·L<sup>-1</sup> NO<sub>2</sub><sup>-</sup>-N MFC (2.57 Ω) and highest in the 120 mg·L<sup>-1</sup> NO<sub>2</sub><sup>-</sup>-N MFC (7.13 Ω). Interestingly, the charge transfer resistance was higher at 30 mg·L<sup>-1</sup> NO<sub>2</sub><sup>-</sup>-N than at 60 mg·L<sup>-1</sup> (3.42 Ω vs. 2.57 Ω).

The effect of influent nitrite concentration on the anode microbial biofilm was assessed by determining the EPS and cytochrome *c* contents on the anode electrode.

As seen in Figs. 4 and 5, both the EPS and cytochrome *c* contents increased as the influent nitrite concentration increased from 0 to 60 mg·L<sup>-1</sup>, peaked at 60 mg·L<sup>-1</sup>, and then substantially declined at higher nitrite concentrations. As these trends were consistent with the power density trend, we determined the regression relations between EPS and power density and between cytochrome *c* and power density. The obtained correlation coefficients were  $r = 0.975$  and  $r = 0.981$ , respectively. The threshold correlation coefficient ( $r_{min}$ ), estimated at the 0.05 significance level of the regression coefficient, was 0.878. Given that  $|r| > r_{min}$  for both EPS and cytochrome *c*, it appears that the nitrite concentration influenced the EPS and cytochrome *c* contents of the anode microorganisms and that the EPS and cytochrome *c* variations were significantly correlated with the system energy output (Herdman and Stapells 2003).

The reduced EPS contents at improperly high nitrite concentrations suggest that excess nitrite decreased the electron transfer rate from the microorganisms to the electrode, thereby lowering the electricity generation. In addition, if most of the substrate was expended in multiplying the microorganisms instead of generating electricity, the electrode surface would be increasingly covered by microbes, inhibiting the electrochemical reaction, increasing the ohmic resistance of the MFC, and reducing its electron transfer efficiency. After 10 days, the initial phase of microbial growth began in the MFC. Accordingly, the charge transfer resistance gradually decreased over time, thus reducing the activation barrier and boosting the output voltage. Our findings agree with Hutchinson et al. (2011), who reported that the charge transfer resistance reduces during biofilm growth before stabilizing with an acclimated biofilm.

As mentioned above, the 60 mg·L<sup>-1</sup> NO<sub>2</sub><sup>-</sup>-N MFC showed the lowest charge transfer resistance (2.57 Ω) during the stable stage of the reactor, implying a relatively high electron transfer efficiency and a more active biofilm than in the other MFCs. In the 30 mg·L<sup>-1</sup> NO<sub>2</sub><sup>-</sup>-N MFC, the charge transfer resistance was 33% higher than in the 60 mg·L<sup>-1</sup> NO<sub>2</sub><sup>-</sup>-N (3.42 Ω vs. 2.57 Ω). This finding is attributed to the relatively low conductivity of the anode electrolyte at the

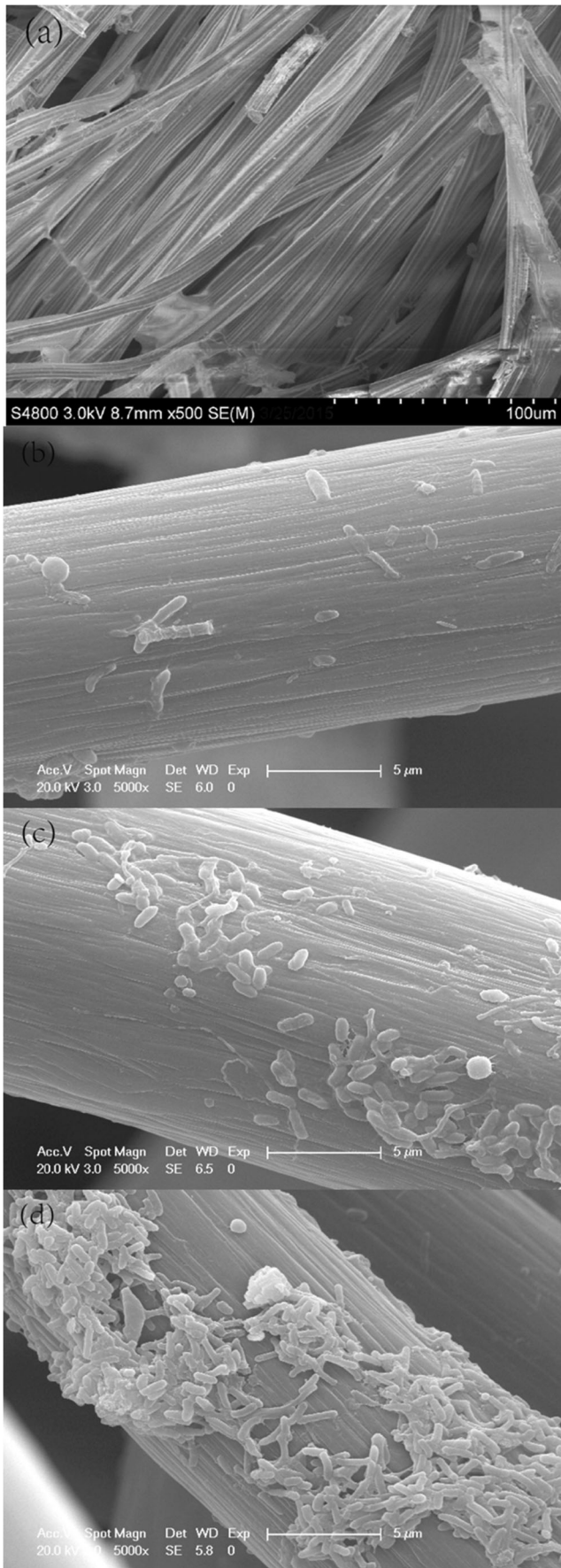


**Fig. 6** Scanning electron micrographs of the anodic biofilm at different stages. The anolytic nitrite concentration was  $60 \text{ mg L}^{-1}$ . (a) Blank carbon felt; (b) Colony formation, 5 days; (c) Biofilm development, 10 d; (days) Biofilm maturation, 25 days

lower nitrite concentration, implying a limited electron transfer. Interestingly, the maximum charge transfer resistance of  $7.13 \Omega$  produced in the  $120 \text{ mg-L}^{-1} \text{NO}_2^- \text{-N}$  MFC was 2.8-fold higher than the  $2.57 \Omega$  produced in the  $60 \text{ mg-L}^{-1} \text{NO}_2^- \text{-N}$  MFC, meaning that high concentrations of additional nitrite inhibited the biofilm growth. This result reflects the biological toxicity of nitrite.

### Surface morphology and biofilm formation

Besides generating internal resistance, microorganisms might crucially affect the performance of an MFC. O'Toole et al. (2000) found that microorganisms undergo profound changes when transitioning from planktonic organisms to cells that are part of a complex, surface-attached community, with

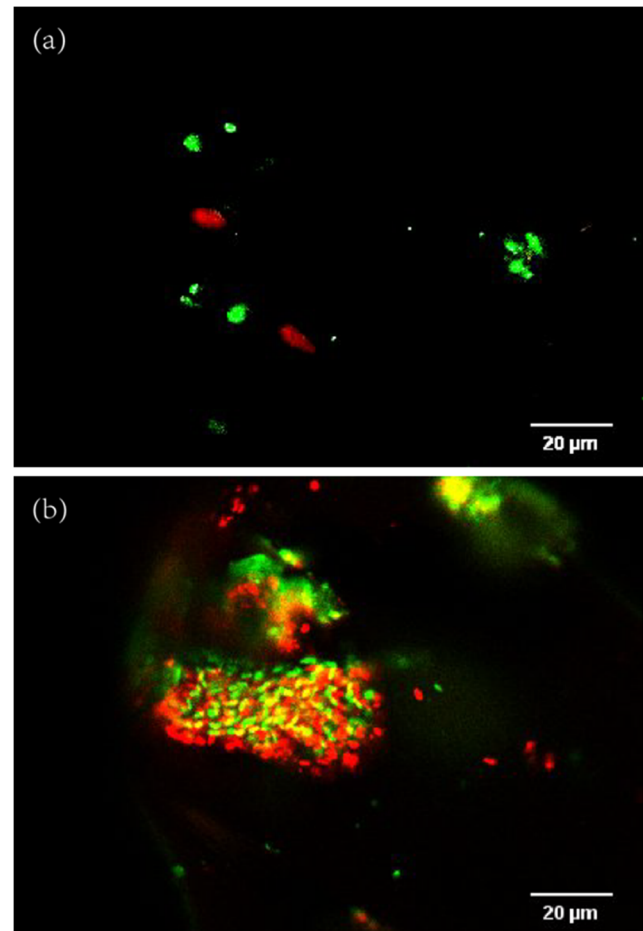


**Fig. 7** Confocal laser scanning micrographs of anodic biofilms at different stages when anolytic nitrite concentration was  $60 \text{ mg L}^{-1}$ . The electrode was stained with LIVE/DEAD BacLight viability stain. (a) Colony formation or the early stage of biofilm growth, 5 days. (b) Biofilm maturation, 25 days

consequent changes in their EPS, internal resistance, and other properties. The biofilm morphologies obtained by SEM and CLSM are presented in Figs. 6 and 7, respectively. The SEM images (Fig. 6a–d) show the growth process of the biofilm on the carbon felt. The biofilm formation process can be divided into three stages: (1) initial attachment and proliferation of bacteria on the electrode surface (initial adhesion), (2) extracellular polymer release (growth), and (3) further adaptation to life in the biofilm after surface attachment (maturation of the biofilm) (O'Toole et al. 2000). Finally, widely diverse organism morphologies are observed on the carbon felt, with rods being the most common morphological form.

The specific composition of the biofilm was elucidated in a CLSM imaging analysis. Figure 7 confirms the rod-shaped form of the organism morphology that dominated the SEM results. Most ( $62.4 \pm 1.2\%$ ) of the biofilm cells maintained were viable during the early stage of biofilm growth, in contrast with the  $52.3 \pm 1.7\%$  biofilm viability at the maturation stage of the biofilm. At this stage, biofilm growth on the electrode was a dynamic equilibrium process, accompanied by the production of new cells and the death of old cells, indicating that the biofilm had stabilized.

EPS, which constitutes mainly carbohydrate and protein, is an important part of the biofilm. The structure and composition of EPS greatly influence the biofilm, and EPS itself promotes the adhesion and growth of microbial cells on the electrode surface (Hamilton 2003). Research has revealed redox-active molecules in EPS, such as outer membrane cytochromes, which facilitate and direct electron transfer. Alternatively, EPS might provide a supporting matrix for the cytochromes and promote their rapid electron transfer (Cao et al. 2011). At influent nitrite concentrations above  $60 \text{ mg}\cdot\text{L}^{-1}$ , the EPS content of the anode biofilm decreased (Fig. 4). Because the EPS contents are closely connected to extracellular electron transfer (Sheng et al. 2010), the lowered EPS may partly account for the increased charge transfer resistance of the system at high nitrite concentrations.

Electron transfer through cytochrome *c* is a primary electronic transfer mode in MFCs (Gralnick and Newman 2007). The heme groups in cytochrome *c* are arranged in a closed space that allows the passage of electrons, facilitating electron transfer from the cells to the outer electrode (Kleerebezem and van Loosdrecht 2007; Mowat and Chapman 2005).

The cytochrome *c* and EPS contents were both relatively high at an influent nitrite concentration of  $60 \text{ mg}\cdot\text{L}^{-1}$  (Figs. 4 and 5). These high levels promoted the electron transfer of microorganisms to the anode electrode, so the charge transfer resistance of the system reduced while the external output voltage increased. The enhanced outside current strengthened the activity of the anode microorganisms, thereby improving their ability to consume organic matters. Moreover, as EPS generation consumes the energy needed for bacterial growth (Qureshi et al. 2005), a large amount of organic matters will be

consumed, so the system coulombic efficiency decreases. At increasingly higher influent nitrite concentrations, the nitrite for microbial growth became increasingly inhibited. Consequently, the EPS and cytochrome *c* contents plummeted, adversely affecting the electricity production capacity of the MFC. However, how the nitrite simultaneously affects the EPS and cytochrome *c* of the electrode biofilm as an electricity-producing matrix needs further investigation.

## Conclusions

A comprehensive analysis of electricity production, nitrogen removal, and surface morphology on an MFC electrode showed that nitrite could react as the co-matrix on the electrode, thereby promoting electricity generation at relatively low concentrations ( $< 60 \text{ mg}\cdot\text{L}^{-1}$  in this study). Higher anolytic nitrite concentration ( $> 60 \text{ mg}\cdot\text{L}^{-1}$ ) inhibited the activity of the electrogenic bacteria, as reflected in the lowered production of cytochrome *c* and EPS, and consequent decrease of the system output voltage. The current output of the MFC was maximized at an anolytic nitrite concentration of  $60 \text{ mg}\cdot\text{L}^{-1}$ ; however, high current also promoted the activity of heterotrophic microorganisms without electricity-producing capacities, thereby decreasing the coulombic efficiency to 5.4%.

**Acknowledgments** This research was supported by the National Key R&D Program of China (2016YFC0400805), the National Natural Science Foundation of China (51878466) and the National Science and Technology Major Project of China on Water Pollution Control and Management (2017ZX07206-001). We also thank the 111 project (B13017) of Tongji University. Dr. Rongchang Wang was supported by the Shanghai Peak Discipline Program at Shanghai Institute of Pollution Control and Ecological Security.

## References

- Al-Mamun A, Baawain MS, Egger F, Al-Muhtaseb AH, Ng HY (2017) Optimization of a baffled-reactor microbial fuel cell using autotrophic denitrifying bio-cathode for removing nitrogen and recovering electrical energy. *Biochem Eng J* 120:93–102
- APHA LS, Clesceri AE, Greenberg AD (1998) Standard methods for the examination of water and wastewater, 20th edn. American Public Health Association, Washington, DC
- Barsoukov E and Macdonald J R (2005) Impedance Spectroscopy: Theory, Experiment, and Applications. Wiley-Interscience, Hoboken.
- Borole AP, Aaron D, Hamilton CY, Tsouris C (2010) Understanding long-term changes in microbial fuel cell performance using electrochemical impedance spectroscopy. *Environ Sci Technol* 44:2740–2745
- Cao B, Shi L, Brown RN, Xiong Y, Fredrickson JK, Romine MF, Marshall MJ, Lipton MS, Beyenal H (2011) Extracellular polymeric substances from *Shewanella* sp. HRCR-1 biofilms: characterization by infrared spectroscopy and proteomics. *Environ Microbiol* 13: 1018–1031



- Chen H, Zheng P, Zhang J, Xie Z, Ji J, Ghulam A (2014) Substrates and pathway of electricity generation in a nitrification-based microbial fuel cell. *Bioresour Technol* 161:208–214
- Ding W, Cheng S, Yu L, Huang H (2017) Effective swine wastewater treatment by combining microbial fuel cells with flocculation. *Chemosphere* 182:567–573
- Fang HH, Xu L, Chan K (2002) Effects of toxic metals and chemicals on biofilm and biocorrosion. *Water Res* 36:4709–4716
- Faraghi N and Ebrahimi S (2012) Nitrite as a candidate substrate in microbial fuel cells. *Biotechnol Lett* 34:1483–1486
- Fu Y, Kok RAW, Dankbaar B, Ligthart PEM, Riel ACR (2018) Factors affecting sustainable process technology adoption: a systematic literature review. *J Clean Prod* 205:226–251
- Gaudy AF (1962) Colorimetric determination of protein and carbohydrate. *Ind Water Wastes* 7:17–22
- Gralnick JA, Newman DK (2007) Extracellular respiration. *Mol Microbiol* 65:1–11
- Hamilton WA (2003) Microbially influenced corrosion as a model system for the study of metal microbe interactions: a unifying electron transfer hypothesis. *Biofouling* 19:65–76
- Herdman AT, Stapells DR (2003) Auditory steady-state response thresholds of adults with sensorineural hearing impairments: Umbral de las respuestas auditivas de estado estable en adultos con hipoacusia sensorineural. *Int J Audiol* 42:237–248
- Hutchinson AJ, Tokash JC, Logan BE (2011) Analysis of carbon fiber brush loading in anodes on startup and performance of microbial fuel cells. *J Power Sources* 196:9213–9219
- Katz E, Willner I (2003) Probing biomolecular interactions at conductive and semiconductive surfaces by impedance spectroscopy: routes to impedimetric immunosensors, DNA-sensors, and enzyme biosensors. *Electroanalysis* 15:913–947
- Kim Y, Shin S, Chang IS, Moon S (2014) Characterization of uncharged and sulfonated porous poly(vinylidene fluoride) membranes and their performance in microbial fuel cells. *J Membr Sci* 463:205–214
- Kleerebezem R, van Loosdrecht MC (2007) Mixed culture biotechnology for bioenergy production. *Curr Opin Biotechnol* 18:207–212
- Logan BE, Regan JM (2006) Electricity-producing bacterial communities in microbial fuel cells. *Trends Microbiol* 14:512–518
- Lowry OH, Rosebrough NJ, Farr AL, Randall RJ (1951) Protein measurement with the Folin phenol reagent. *J Biol Chem* 193:265–275
- Lu H, Oehmen A, Virdis B, Keller J, Yuan Z (2006) Obtaining highly enriched cultures of *Candidatus Accumulibacter phosphatus* through alternating carbon sources. *Water Res* 40:3838–3848
- Ma B, Yang L, Wang Q, Yuan Z, Wang Y, Peng Y (2017) Inactivation and adaptation of ammonia-oxidizing bacteria and nitrite-oxidizing bacteria when exposed to free nitrous acid. *Bioresour Technol* 245(Pt A):1266–1270
- Magnussen BF, Hjertager BW (1981) On the structure of turbulence and a generalized eddy dissipation concept for chemical reaction in turbulent flow 19th AIAA aerospace meeting, St. Louis, USA
- McCarty P L, Bae J, Kim J (2011) Domestic wastewater treatment as a net energy producer—can this be achieved? *Environmental Science and Technology*, 45(17):7100–7106.
- Moharir PV, Tembhurkar AR (2018) Effect of recirculation on bioelectricity generation using microbial fuel cell with food waste leachate as substrate. *Int J Hydrog Energy* 43(21):10061–10069
- Mowat CG, Chapman SK (2005) Multi-heme cytochromes—new structures, new chemistry. *Dalton Trans* 3381–3389
- Oh ST, Kim JR, Premier GC, Lee TH, Kim C, Sloan WT (2010) Sustainable wastewater treatment: how might microbial fuel cells contribute. *Biotechnol Adv* 28:871–881
- O'Toole G, Kaplan HB, Kolter R (2000) Biofilm formation as microbial development. *Annu Rev Microbiol* 54:49–79
- Park Y, Nguyen VK, Park S, Yu J, Lee T (2018) Effects of anode spacing and flow rate on energy recovery of flat-panel air-cathode microbial fuel cells using domestic wastewater. *Bioresour Technol* 258:57–63
- Qureshi N, Annous BA, Ezeji TC, Karcher P, Maddox IS (2005) Biofilm reactors for industrial bioconversion processes: employing potential of enhanced reaction rates. *Microb Cell Factories* 4:24
- Sheng G, Yu H, Li X (2010) Extracellular polymeric substances (EPS) of microbial aggregates in biological wastewater treatment systems: a review. *Biotechnol Adv* 28:882–894
- Sinclair PR, Gorman N, Jacobs JM (2001) Measurement of heme concentration. *Curr Protoc Toxicol* 8(3):1–8.3.7
- Sun G, Thygesen A, Ale MT, Mensah M, Poulsen FW, Meyer AS (2014) The significance of the initiation process parameters and reactor design for maximizing the efficiency of microbial fuel cells. *Appl Microbiol Biotechnol* 98:2415–2427
- Virdis B, Harnisch F, Batstone DJ, Rabaey K, Donose BC (2012) Non-invasive characterization of electrochemically active microbial biofilms using confocal Raman microscopy. *Energy Environ Sci* 5: 7017–7024
- Virdis B, Rabaey K, Rozendal R A, Yuan Z, Keller J (2010) Simultaneous nitrification, denitrification and carbon removal in microbial fuel cells. *Water Research*, 2010, 44(9):2970–2980

**Publisher's note** Springer Nature remains neutral with regard to jurisdictional claims in published maps and institutional affiliations.